J Supercond Nov Magn (2017) 30:763–768
DOI 10.1007/s10948-016-3644-6

ORIGINAL PAPER

Anisotropic Superconducting Gaps and Boson Mode in $FeSe_{1-x}S_x$ Single Crystals

C. Di Giorgio[1] · A. V. Putilov[1] · D. J. Trainer[1] · O. S. Volkova[2,3,4] · A. N. Vasiliev[2,3,4] · D. Chareev[3,5] · G. Karapetrov[6] · J. F. Zasadzinski[7] · M. Iavarone[1]

Received: 9 May 2016 / Accepted: 19 July 2016 / Published online: 20 August 2016

Abstract Scanning tunneling spectroscopy has been used to investigate the superconducting gaps of $FeSe_{1-x}S_x$ single crystals and to reveal signatures of a bosonic mode in the quasiparticle density of states. We find that both superconducting gaps residing on different pockets of the Fermi surface are anisotropic. Moreover, the bosonic mode appears in the quasiparticle density of states as a redistribution of states at energy Ω/e, measured with respect to the superconducting gap. The energy of the boson mode Ω is found to scale with the superconducting gap, and it can be estimated to be in the range 2.6 ÷ 3.8 meV in agreement with a recent observation of a resonance spin excitation in neutron scattering. This suggests that quasiparticle interactions with this mode are important for superconductivity.

Keywords Superconducting materials-chalcogenides · Electronic structure · Scanning tunneling microscopy · Tunneling

1 Introduction

FeSe has the simplest crystal structure among the Fe-based superconductors. It exhibits a structural transition from tetragonal to orthorhombic at T_s ∼90 K [1] and a superconducting critical temperature at T_c ∼9 K [2]. Below T_s, a strong electronic anisotropy of the Fermi surface has been observed by angle-resolved photoemission spectroscopy [3] that cannot be explained in terms of the difference in the lattice parameters (only 0.1 %). Therefore, this phase is driven by an electronic degree of freedom, namely the electronic nematic order [4]. The origin of this symmetry breaking is currently one of the most intensely debated issues in the literature. It has been proposed that nematicity could be driven either by orbital ordering of the Fe d electrons or by spin fluctuations. Furthermore, orbital ordering would favor a sign preserving s-wave superconducting order parameter [5, 6] while spin fluctuations would favor a sign changing $s\pm$ or d-wave pairing [7]. Different from Fe-based pnictides, no long-range order magnetic phase has been observed in this material, which provides the opportunity to study the nematic phase down to the superconducting state.

Tunneling spectroscopy is a powerful technique that not only allows to reveal the superconducting gap but also provides important information on the symmetry of the order parameter through the changes of the local density

✉ M. Iavarone
iavarone@temple.edu

1 Physics Department, Temple University, Philadelphia, PA 19122, USA

2 Physics Faculty, M.V. Lomonosov Moscow State University, Moscow, 119991, Russia

3 Institute of Physics and Technology, Ural Federal University, Yekaterinburg, 620002, Russia

4 National University of Science and Technology "MISiS", Moscow, 119049, Russia

5 Institute of Experimental Minerology, Russian Academy of Sciences, Chernogolovka, Moscow District, 142432, Russia

6 Physics Department, Drexel University, Philadelphia, PA 19104, USA

7 Physics Department, Illinois Institute of Technology, Chicago, IL 60616, USA

of states at defect sites [8, 9], while superconducting gaps on different portions of the Fermi surface can be detected by directional tunneling [10]. The superconducting gaps in this material have been measured by scanning tunneling microscopy and scanning tunneling spectroscopy (STM/STS) on thin films [11] and single crystals [9, 12], planar junction [13], and point contact spectroscopy [14]. Some of the features in the tunneling spectra have been observed in all experiments, while others have appeared with different strengths depending upon the sample, geometry of the experiment (planar vs STM), and temperature, making, therefore, the interpretation of these features still controversial. Moreover, different from other Fe-based superconductors, with higher T_c and bigger gaps, angle-resolved photoemission cannot adequately resolve these small gaps on different portions of the Fermi surface. Only a recent report on the angle-resolved photoemission study of $FeSe_{0.93}S_{0.07}$ shows a pronounced twofold anisotropy of the superconducting gap at the hole pocket, while no gap was observable on the electron pocket [15].

Furthermore, tunneling experiments can reveal a signature of the boson mode that couples electrons in the superconducting state from the deviation of the tunneling spectrum from the Bardeen-Cooper-Schrieffer (BCS) theory of superconductivity, and therefore provide important information on the pairing mechanism. Indeed, soon after Giaever succeeded in experimentally revealing the energy gap in the quasiparticle density of states of superconducting Pb in a tunneling experiment [16], he also observed additional fine structure outside the coherence peaks [17, 18]. The deviations from the smooth BCS shape reflect the energy-dependent gap function affected by the phonons as consistently described by the Eliashberg strong-coupling theory [19]. The most prominent features produced by a single phonon mode at Ω in the quasiparticle density of states of a superconductor is a strong decrease very close to $\Delta + \Omega$, symmetrically for occupied and unoccupied states. Furthermore, since the strong-coupling phonon features arise from the energy-dependent gap function, their intensity is expected to decrease as the temperature is raised and to vanish at the critical temperature. In recent years, reports on the observation of dip-hump features outside the gap in tunneling spectra obtained by STM/STS and break junction measurements on different cuprates [20–23] and iron-based superconductors [24] were published. They have been interpreted as a manifestation of a bosonic mode similar to strong-coupling effects in conventional superconductors [25–27]. In the case of unconventional superconductors, it is usually supposed that the origin of the bosonic mode is spin excitations rather than phonons. This hypothesis is based on the agreement of the mode energy extracted from the tunneling spectrum with the energy of spin excitation measured by inelastic neutron scattering.

In this paper, we report scanning tunneling microscopy and spectroscopy measurements performed on $FeSe_{1-x}S_x$ single crystals and we provide the first directional tunneling that shows the presence of two anisotropic gaps. Moreover, we clearly observe the boson mode feature in tunneling spectra of $FeSe_{1-x}S_x$ with different S contents, where variations of the gaps with tunneling direction, in proximity of twin boundaries and in samples with different S substitution levels, allow to correlate the strength of the boson mode with the superconducting gap.

2 Samples

$FeSe_{1-x}S_x$ single crystals were grown in evacuated quartz ampoules using the $AlCl_3$/KCl flux technique in a temperature gradient (from 400 to ∼50 °C) for 45 days [28]. The chemical composition of crystals was studied with a digital scanning electron microscope (TESCAN Vega II XMU) [28]. The standard deviation of the average S concentration gives an indication of the homogeneity of S within the crystals. Therefore, the composition and, in particular, the S concentration level were obtained by averaging over several different points of each single crystal. The analysis showed that the approximate chemical compositions are $FeSe_{1-\delta}$ ($x = 0$), $Fe(Se_{0.96\pm0.01}S_{0.04\pm0.01})_{1-\delta}$ ($x = 0.04$), and $Fe(Se_{0.91\pm0.01}S_{0.09\pm0.01})_{1-\delta}$ ($x = 0.09$) (δ represents the Se vacancies naturally present in these samples) and that the samples are of high-quality tetragonal β-FeSe phase as described in detail elsewhere [13]. The superconducting critical temperatures are 8.5, 9.6, and 10.1 K for $x = 0$, 0.04, and 0.09, respectively [9].

3 Results

Lowtemperature STM/STS measurements were performed at $T = 1.5$ K, using the Unisoku UHV STM system, with a base pressure of 4×10^{-11} Torr. All samples were cleaved in UHV at room temperature and, after, were soon transferred to the STM at low temperature. Pt-Ir tips were used in all measurements.

In the limit of low temperature and voltages, the tunneling conductance (dI/dV vs V) between a normal tip and a sample is proportional to the local electronic density of states of the sample. Tunneling spectroscopy was performed using the standard lock-in technique with an ac modulation of 0.2 mV at 373 Hz. The atomically resolved topographic images were acquired in the constant current mode.

Figure 1a–c shows the representative atomic resolution STM topography images acquired at the surface of $FeSe_{1-x}S_x$ crystals with different S contents. The S atoms are associated with dark spots in the images, consistent with

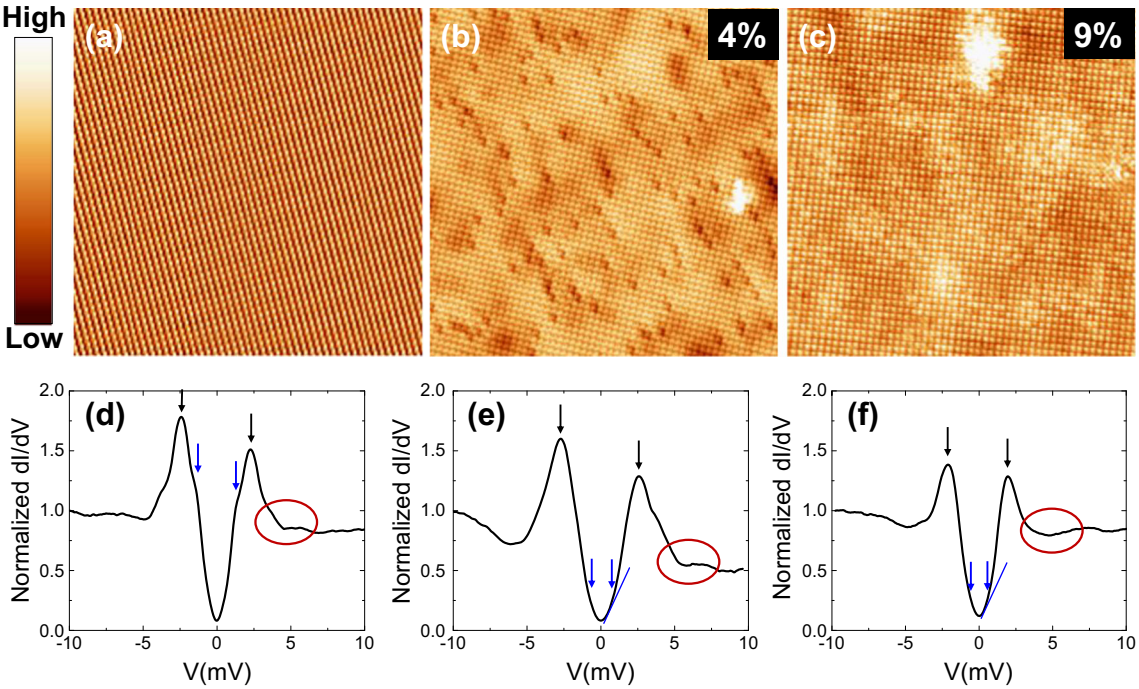

Fig. 1 **a–c** Representative atomic resolution STM topography images acquired on the surface $FeSe_{1-x}S_x$ single crystals with $x = 0$, $x = 0.04$, and $x = 0.09$, respectively. Scanning conditions are $V = 20$ mV and $I = 100$ pA. The scan areas for all images are 19.6 nm × 19.6 nm. **d–f** Representative tunneling spectra for the samples $x = 0$, $x = 0.04$, and $x = 0.09$, respectively. All spectra were acquired at $T = 1.5$ K, and they were normalized by the tunneling conductance at $V = -10$ mV. The *arrows* point at the main coherence peak (higher energy feature) and at a kink observed in all spectra (at lower energy). The *circled region* highlights the deviations from the BCS that will be discussed in Fig. 3

the nominal S content. Representative tunneling spectra for pure ($x = 0$), $x = 0.04$, and $x = 0.09$ samples acquired at $T = 1.5$ K are shown in Fig. 1d–f. The spectrum acquired on the pure sample (Fig. 1d) is V-shaped (consistent with nodes in the gap) and shows clear coherence peaks at ± 2.3 meV. These peaks can be tracked in temperature up to the critical temperature $T_c = 8.5$ K. The obtained values of Δ and T_c yield $\frac{2\Delta}{k_B T_c} \approx 6.3$ much higher than the BCS ratio and place this material in the strong-coupling limit. Other two features appear symmetrically at ±1.3 meV, and they are more evident at 0.4 K [9]. Since tunneling integrates the gap in momentum space, it is difficult from these data alone to establish the origin of this feature. It might arise 162 from a strongly anisotropic gap on the Γ pocket, or it could be related to the gap on the M pocket. Based on the density functional theory, these tunneling spectra are consistent with different explanations of their origin [29, 30]. Without a clear model, it is not possible to determine the temperature dependence of the low-energy features since they are not clearly visible from the tunneling spectra already at 2 K. The temperature dependence of the two gaps is governed by the interband coupling that is supposed to be quite weak in FeSe [31]. Finally, a third feature appearing symmetrically at energy above the gap has been associated with a boson mode feature [32] and it will be discussed in detail in Fig. 3.

The same features are also present in the tunneling spectra acquired on the sample with $x = 0.04$. In this case, the main pair of symmetric peaks moves at ±2.6 meV consistent with an increase of T_c to 9.6 K and the low-energy feature moves at 0.7 meV. In the case of $x = 0.09$, the main pair of peaks moves at lower energy ±2 meV and it anti-correlates with $T_c = 10.1$ K. The simultaneous decrease in the gap and increase in T_c are only possible in a multigap scenario. It can indeed be related either to an increase of interband scattering or to a change in band structure with consequent changes in holes and electron concentration.

In Fig. 2a, a topographic image acquired at the surface of a pure FeSe crystal (without S substitution) is reported. The image shows a step with the atomic lattice continuous along the step and no indication of a twin boundary or a stressed lattice. In Fig. 2b, a sequence of tunneling spectra recorded across the step is shown. The position labeled as $x = 0$ indicates the middle of the step. The tunneling spectra change across the step. In the middle of the step, a clear two-gap feature emerges (Fig. 2e) that is not present when tunneling along the *c*-axis (Fig. 2d) of the crystal structure of the sample. In order to explain these results, details of the band structure need to be taken into account and the signature of the band structure effects in a tunneling experiment needs to be addressed. According to angle-resolved photoemission

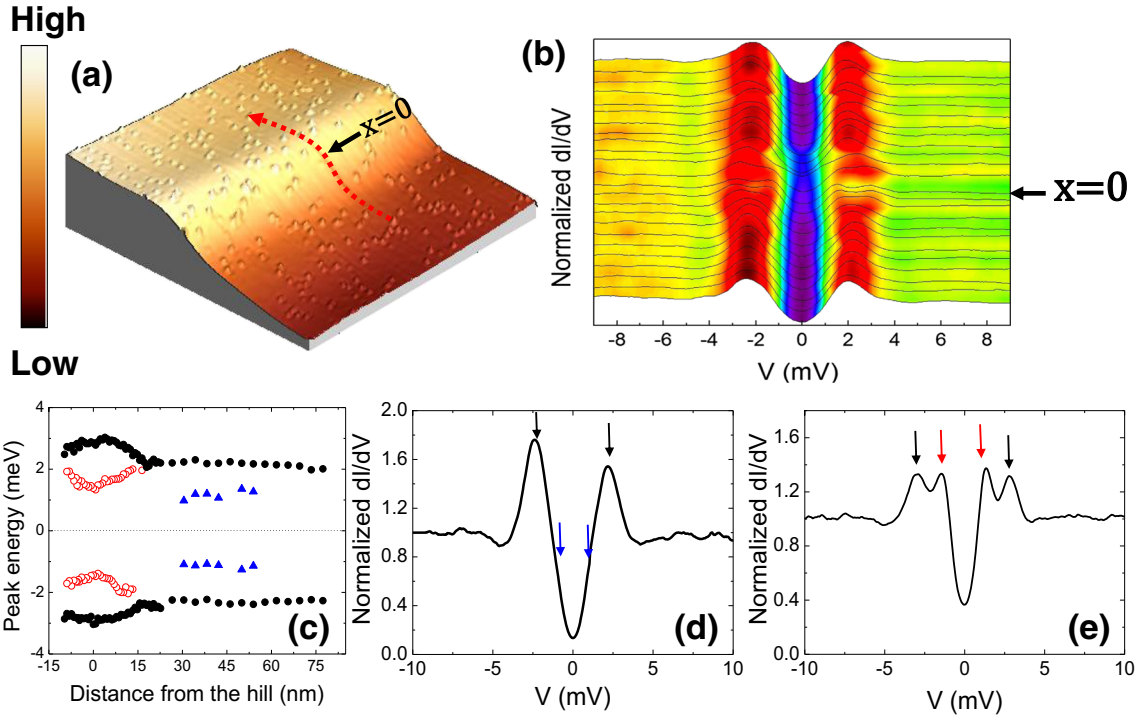

Fig. 2 **a** STM topography image acquired on the surface of a pure FeSe ($x = 0$) single crystal and showing a step-like feature. The defects in the image correspond quite likely to Se deficiencies in the crystal. The image has been acquired at $V = 20$ mV and $I = 100$ pA. The scan area is 312.5 nm × 312.5 nm. **b** Sequence of tunneling spectra acquired across the step (*line* in *a*) at $T = 1.5$ K. Tunneling parameters are $V = 10$ mV and $I = 100$ pA. **c** Plot of the gaps as a function of the distance from the center of the step ($x = 0$). The filled circles are the large energy peaks, the triangles are the features that appear as kinks in the tunneling spectra when tunneling along the *c*-axis (Fig. 2d, kinks at low energy are indicated by arrows), while the open circles are the low-energy peaks that appear clearly on the step (Fig. 2e). The triangles have been obtained from the first derivative of the *dI/dV*. **d** Typical tunneling spectrum acquired on the c-axis regions. The arrows indicate the features that are summarized in c with filled and open circles, respectively. **e** Typical tunneling spectrum recorded on the step. The *black* and *red arrows* indicate the features summarized in *c* with *black* and *red dots*, respectively

measurements, the Fermi surface of FeSe consists of one hole pocket at the Γ point and one electron pocket at the M point [3]. Theory and quantum oscillation experiments reveal a second pocket at the M point as well [33]. Two different energy gaps might exist on different portions of the Fermi surface. To understand how such a highly anisotropic band structure can manifest itself in a tunneling experiment, the tunneling matrix element has to be considered. Indeed, although the tunneling matrix element is considered to be constant in the conventional treatment of tunneling, there is a factor $D(\mathbf{k})$ that is proportional to the quasiparticle's group velocity (v_g) and the directionality function that needs to be taken into account. The tunneling matrix element can be written as $|T^2| = v_g D(\mathbf{k})$ where v_g is the quasiparticle group velocity ($v_g = |\nabla_k \varepsilon_k \cdot \mathbf{n}|$) and $D(\mathbf{k})$ is the directionality function. The directionality function has the form [34]

$$D(\mathbf{k}) = \exp\left(\frac{k^2 - (k \cdot \mathbf{n})^2}{(k \cdot \mathbf{n})^2 \Theta_0^2}\right)$$

where $\mathbf{n}$ defines the tunneling direction perpendicular to the surface of the sample and Θ_0 is the tunneling cone spread in k space of the quasiparticle momenta with non-negligible tunneling probability with respect to $\mathbf{n}$. For $\Theta_0 \ll 1$, only the quasiparticle with momenta very close to the direction of $\mathbf{n}$ has significant tunneling probability; i.e., the theory of tunneling strongly favors transitions with k perpendicular to the surface, into a cone with an opening angle of $5° \pm 10°$. In the case of FeSe, similar to the case of MgB_2 [10, 35–37] due to the highly anisotropic band structure, different tunneling directions should probe different bands at the Fermi surface with corresponding weights depending upon the tunneling direction. In particular, tunneling along the *c*-axis direction of the crystalline structure of FeSe tunneling should selectively probe preferentially the Γ pocket, while tunneling at different angles increases the probability of tunneling into the M pocket.

Moving the tip across the step corresponds to tunneling at an angle Θ_0 with the *c*-axis crystallographic direction increasing then the probability to tunnel into the M pocket. In Fig. 2c, the summary of the peak position as a function of location is reported. The filled circles represent the values of the higher energy gap, the open circles represent the values of the low-energy gap in spectra like those in

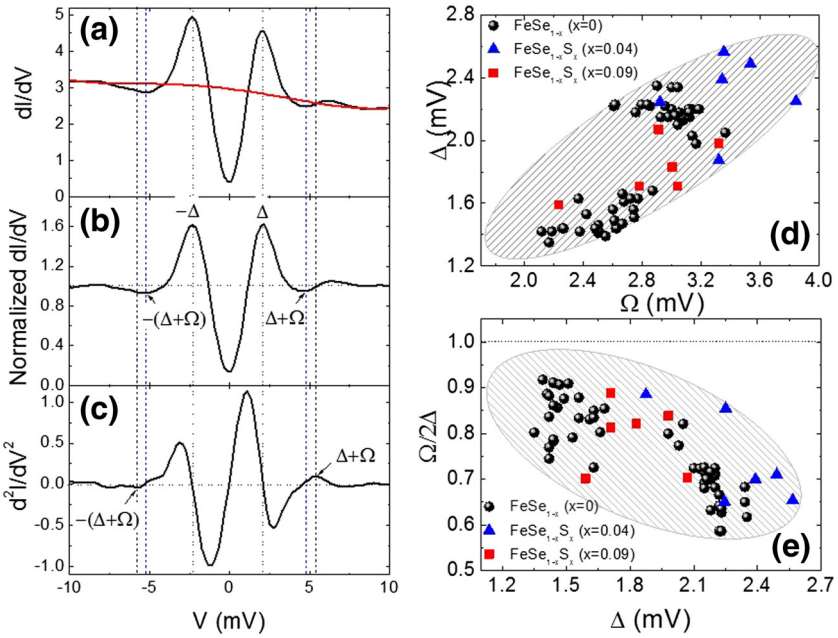

Fig. 3 **a** Characteristic tunneling spectrum acquired at $T = 1.5$ K, with $V = 10$ mV and $I = 100$ pA, shown together with the curve to which the spectrum has been normalized to. The result of the normalization is reported in **b**. **c** The first derivative of the dI/dV spectrum. The *two dashed lines* describe the two methods used to determine the $\Delta + \Omega$ feature from the tunneling spectra. **d** Dependence of the superconducting gap on the bosonic mode energy Ω at $T = 1.5$ K. **e** $\Omega/2\Delta$ plotted as a function of Δ. Note that $\Omega/2\Delta$ remains below 1 for the collected data

Fig. 2e, while the triangles represent the position of the kink at lower energy in spectra like those in Fig. 2d (derived from the first derivative of the *dI*/*dV*). This summary plot clearly shows the existence of two anisotropic gaps on both hole and electron pockets in FeSe.

In Fig. 3, we focus on the boson mode revealed by tunneling spectra. The spectra acquired along the step and in samples with different S contents provide a wide range of gap values and allow us to correlate the energy of the boson mode with gap values.

Figure 3a shows the tunneling spectrum acquired on a pure sample at $T = 1.5$ K.

To analyze the tunneling spectra, we first normalize it as shown in Fig. 3a, and b. The normalization curve is either the normal state conductance curve acquired at a temperature higher than T_c or the polynomial fit of the conductance curve in the superconducting state that excludes the part of the spectrum close to the Fermi level. The value of the energy gap Δ is chosen at the energy corresponding to the main coherence peaks. The position of $\Delta + \Omega$, where Ω is the boson mode, in a single-band Eliashberg theory, is at the minimum of the dip for a *d*-wave order parameter and at the inflection point for an *s*-wave order parameter [38]. The inflection point is determined by taking the derivative of the *dI*/*dV* curve. The maximum at positive bias and the minimum at negative bias outside the coherence peaks in the d^2I/dV^2 spectrum represent the location of $\pm(\Delta + \Omega)$ (Fig. 3c). To determine Ω correctly, one would need to fit the data with a two-gap Eliashberg theory for strongly coupled superconductors. Here, we determine this position by determining both the minimum and inflection point and then by plotting the average between the two. The error on the determination of Ω has been estimated to vary between 0.2 and 0.5 meV. In Fig. 3d, we plot the obtained values of Ω as a function of Δ and we show that Ω correlates with Δ. The points in Fig. 3d have been obtained either on different samples or on the same sample at different locations, where changes of the gap value are due to different tunneling directions or defects. The energy of the boson mode Ω ranges between 2.6 and 3.8 meV in our data and yield a $\Omega/k_BT_c \approx 4 \div 5$ similar to other Fe-based superconductors [39]. According to the Eliashberg theory, the energy of such excitation should remain below the pair-breaking energy, namely $\Omega/2\Delta < 1$ [40]. In Fig. 3e, we demonstrate that this ratio is always below 1 in our data.

4 Discussion and Conclusions

We have investigated the aspects of the multiband superconductivity in FeSe single crystals and the boson mode in tunneling spectra.

Different gap amplitudes can be present on different portions of the Fermi surface similar to the case of MgB_2 [41]. With tunneling spectroscopy, it is possible to probe different pockets by tunneling into different crystallographic directions of the sample. We found that a larger anisotropic gap (accessible when tunneling along the *c*-axis of the sample) resides on the Γ hole pocket of FeSe while a smaller anisotropic gap on the electron pocket at the M point. The main results are summarized in Fig. 2. In particular in Fig. 2c, there is a summary of the different features observed while tunneling in FeSe from different directions.

Moreover, a feature in the tunneling spectrum at energy higher than the gap has been associated to either a boson mode [32] or a signature of another gap [12]. We have

analyzed the tunneling spectra with different values of the energy gap (due to tunneling in different directions and different sulfur substitution levels), and we have observed that this feature scales with the energy gap. This feature that disappears with T_c is similar to structures ascribed to a phonon mode interacting with quasiparticles in conventional superconductors and suggest that the electrons are coupled to some type of collective excitation of energy Ω. More importantly, we find that the energy scale of this feature in the tunneling spectra is comparable to a spin resonant mode found in neutron scattering [42]. Therefore, this strongly suggests that spin fluctuations play an important role in the pairing mechanism of FeSe.

Acknowledgments The work at Temple University (where low-temperature STM was performed) was supported by the US Department of Energy, Office of Basic Energy Sciences, Division of Materials Sciences and Engineering under Award DE-SC0004556. The work at Drexel University and at M.V. Lomonosov Moscow State University was supported by Award Nos. FSAX-14-60108-0 and OISE-14-60109-0 of the US Civilian Research and Development Foundation (CRDF). The work in Russia was supported in part by the Ministry of Education and Science of the Russian Federation in the framework of Increase Competitiveness Program of the NUST "MISiS" (Grant No. K4-2015-020). One of the authors (C.D.G.) would like to acknowledge the partial support from the MIUR (Ministry of Education, Universities and Research of the Italian Government).

References

1. McQueen, T.M., Williams, A.J., Stephens, P.W., Tao, J., Zhu, Y., Ksenofontov, V., Casper, F., Felser, C., Cava, R.J.: Phys. Rev. Lett. **103**, 057002 (2009)
2. Hsu, F.C., et al.: Proc. Natl. Acad. Sci. USA **105**, 14262 (2008)
3. Watson, M.D., et al.: Phys. Rev. B **91**, 155106 (2015)
4. Fernandes, R.M., Chbukov, A.V., Schmalian, J.: Nat. Phys. **10**, 97 (2014)
5. Kontani, H., Onrai, S.: Phys. Rev. Lett. **104**, 157001 (2010)
6. Yanagi, Y., Yamakawa, Y., Ono, Y.: Phys. Rev. B **81**, 054518 (2010)
7. Mazin, I.I., Singh, D.J., Johannes, M.D., Du, M.H.: Phys. Rev. Lett. **101**, 057003 (2008)
8. Song, C.-L., Hoffman, J.E.: Curr. Opin. Solid State Mater. Sci. **17**(2), 39 (2013)
9. Moore, S.A., Curtis, J.L., Di Giorgio, C., Lechner, E., Abdel-Hafiez, M., Volkova, O.S., Vasiliev, A.N., Chareev, D.A., Karapetrov, G., Iavarone, M.: Phys. Rev. B **92**, 235113 (2015)
10. Iavarone, M., Karapetrov, G., Koshelev, A.E., Kwok, W.K., Crabtree, G.W., Hinks, D.G., Kang, W.N., Choi, E.-M.i., Kim, H.J., Kim, H.J., Lee, S.I.: Phys. Rev. Lett. **89**, 187002 (2002)
11. Song, C.-L., Wang, Y.-L., Jiang, Y.-P., Zhi, L., Wang, L., He, K., Chen, X., Hoffman, J.E., Ma, X.-C., Xie, Q.-K.: Science **332**, 1410 (2011)
12. Kasahara, S., Watashige, T., Hanaguri, T., Kohsaka, Y., Yamashita, T., Shimoyama, Y., Mizukami, Y., Endo, R., Ikeda, H., Aoyama, K., Terashima, T., Uji, U., Wolf, T., Löhneysen, V.H., Shibauchi, T., Matsuda Y.: Proc. Natl. Acad. Sci. USA **111**, 16309 (2014)
13. Venzmer, E., Kronenberg, A., Jourdan, M.: arXiv:1506.01877
14. Ponomarev, Y.G., et al.: J. Supercond. Nov. Magn. **26**, 2867 (2013)
15. Xu, H.C., Niu, X.H., Xu, D.F., Jiang, J., Yao, Q., Abdel-Hafiez, M., Chareev, D.A., Vasiliev, A.N., Peng, R., Feng, D.L.: arXiv:1603.05219v1 (2016)
16. Giaver, I.: Phys. Rev. Lett. **5**, 147 (1960)
17. Giaver, I., Hart, H.R., Megerle, K.: Phys. Rev. **126**, 941 (1962)
18. Giaver, I.: Science **183**, 1253 (1974)
19. Rowell, J.M., Anderson, P.W., Thomas, D.E.: Phys. Rev. Lett. **10**, 334 (1963)
20. De Wilde, Y., Miyakawa, N., Guptasarma, P., Iavarone, M., Ozyuzer, L., Zasadzinski, J.F., Romano, P., Hinks, D.G., Kendziora, C., Crabtree, G.W., Gray, K.E.: Phys. Rev. Lett. **80**, 153 (1998)
21. Zasadzinski, J.F., Ozyuzer, L., Miyakawa, N., Gray, K.E., Hinks, D.G., Kendziora, C.: Phys. Rev. Lett. **87**, 067005 (2001)
22. Fisher, Ø., Kugler, M., Maggio-Aprile, I., Berthod, C., Renner, C.: Rev. Modern Phys. **79**, 353 (2007)
23. Niestemski, F.C., Kunwar, S., Zhou, S., Li, S., Ding, H., Wang, Z., Dai, P., Madhavan, V.: Nature **450**, 1058 (2007)
24. Song, C.-L., Hoffman, J.E.: Current opinion in solid state and materials. Science **17**, 39 (2013)
25. Ahmadi, O., Coffey, L., Zasadzinski, J.F.: Phys. Rev. Lett. **106**, 167005 (2011)
26. Shan, L., Gong, J., Wang, Y.-L., Shen, B., Hou, X., Ren, C., Yang, H., Wen, H.-H., Li, S., Dai, P.: Phys. Rev. Lett. **108**, 227002 (2012)
27. Wang, Z., Yang, H., Fang, D., Shen, B., Wang, Q.-H., Shan, L., Zhang, C., Dai, P., Wen, H.-H.: Nat. Phys. **9**, 42 (2013)
28. Chareev, D., Osadchii, E., Kuzmicheva, T., Lin, J.Y., Kuzmichev, S., Volkova, O., Vasiliev, A.: Cryst. Eng. Comm. **15**, 1989 (2013)
29. Mukherjee, S., Kreisel, A., Hirschfeld, P.J., Andersen, M.: Phys. Rev. Lett. **115**, 026402 (2015)
30. Kreisel, A., Mukherjee, S., Hirschfeld, P.J., Andersen, M.: Phys. Rev. B **92**, 224515 (2015)
31. Komendová, L., Chen, Y., Shanenko, A.A., Milošević, M.V., Peeters, F.M.: Phys. Rev. Lett. **108**, 207002 (2012)
32. Song, C.L., Wang, Y.L., Jiang, Y.P., Li, Z., Wang, L.L., He, K., Chen, X., Hoffman, J.E., Ma, X.C., Xue, Q.K.: Phys. Rev. Lett. **112**(5), 057002 (2014)
33. Terashima, T., et al.: Phys. Rev. B **90**, 144517 (2014)
34. Yusof, Z., Zasadzinski, J.F., Coffey, L., Miyataka, N.: Phys. Rev. B **58**, 514 (1998)
35. Iavarone, M., Karapetrov, G., Koshelev, A.E., Kwok, W.K., Crabtree, G.W., Kang, W.N., Choi, E.-M., Kim, H.J., Lee, S.-I.: Supercond. Sci. Technol. **17**, S106 (2004)
36. Szabó, P., Samuely, P., Kačmarčík, J., Klein, T., Marcus, J., Fruchart, D., Miraglia, S., Marcenat, C., Jansen, A.G.M.: Phys. Rev. Lett. **87**(13), 137005 (2001)
37. Giubileo, F., Roditchev, D., Sacks, W., Lamy, R., Thanh, D.X., Klein, J., Miraglia, S., Fruchart, D., Marcus, J.: Phys. Rev. Lett. **87**(17), 177008 (2001)
38. Romano, P., Ozyuzer, L., Yusof, Z., Kurter, C., Zasadzinski, J.F.: Phys. Rev. B **73**, 092514 (2006)
39. Wang, Z., Yang, H., Fang, D., Shen, B., Wang, Q.-H., Shan, L., Zhang, C., Dai, P., Wen, H.-H.: Nat. Phys. **9**, 42 (2012)
40. Eschrig, M.: Adv. Phys. **55**, 47 (2006)
41. Milošević, M.V., Perali, A.: Supercond. Sci. Technol. **28**, 060201 (2015)
42. Wang, Q., Shen, Y., Pan, B., Hao, Y.Q., Ma, M.W., Zhou, F., Steffens, P., Schmalzl, K., Forrest, T.R., Abdel-Hafiez, M., Chen, X.J., Chareev, D.A., Vasiliev, A.N., Bourges, P., Sidis, Y., Cao, H.B., Zhao, J.: Nat. Mater. **15**(2), 159 (2016)

Cinzia Di Giorgio's present address is E.R. Caianiello Physics Department and NANOMATES, Research Centre for Nanomaterials and Nanotechnology, University of Salerno, Fisciano (SA), Italy.